Synaptic inhibition of Purkinje cells mediates consolidation of vestibulo-cerebellar motor learning

Peer Wulff, Martijn Schonewille, Massimiliano Renzi, Laura Viltono,
Marco Sassoè-Pognetto, Aleksandra Badura, Zhenyu Gao, Freek E Hoebeek,
Stijn van Dorp, William Wisden, Mark Farrant and Chris I De Zeeuw

Supplementary Material – Figures and Data

Nature Neuroscience: doi:10.1038/nn.2348

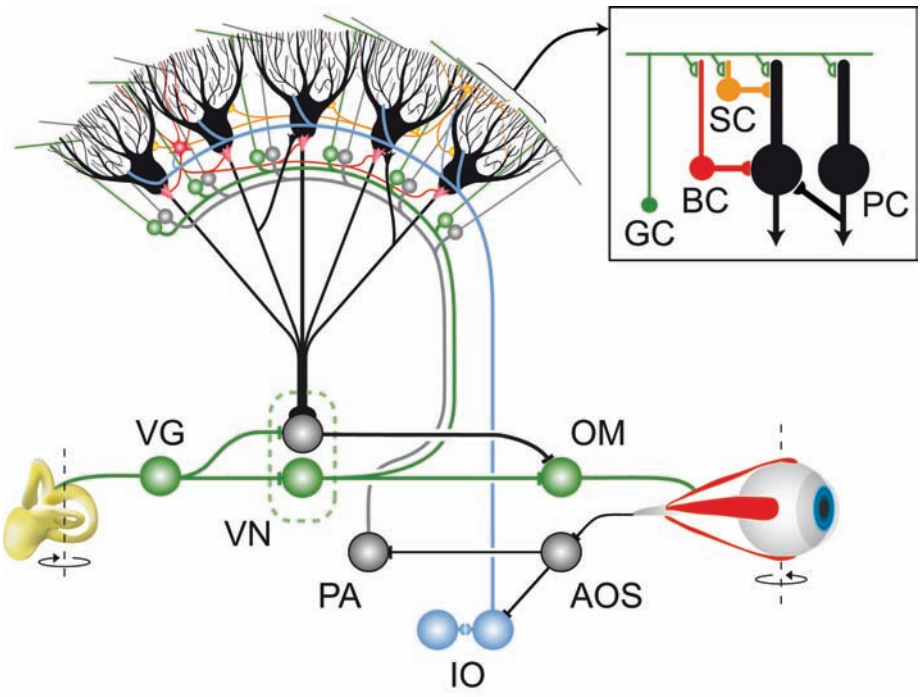

Figure S1 Connectivity of interneurons in the molecular layer of the cerebellar cortex and their relationship to the vestibulo-ocular system. Purkinje cells (PC; black) in the flocculus of the vestibulo-cerebellum converge upon neurons in the vestibular nuclei (VN), through which they can influence the output of the oculomotor neurons (OM) that drive the eye movements. The Purkinje cells receive vestibular and eye movement signals through the mossy fiber-parallel fiber system (green and grey inputs, respectively), and retinal slip signals through the climbing fibers derived from the inferior olive (IO; blue). The parallel fibers, which all originate from the granule cells (GC), innervate the dendritic trees of both Purkinje cells and molecular layer interneurons (basket cells, BC: red and stellate cells, SC: orange), thereby providing a feed-forward inhibitory connection (inset). The axons of both basket and stellate cells are oriented in the same sagittal plane as that of the dendritic trees of Purkinje cells. Some Purkinje cells also receive inhibition via axon collaterals from neighbouring Purkinje cells. VG, AOS and PA indicate vestibular ganglion cells, accessory optic system, and pontine areas, respectively.

Nature Neuroscience: doi:10.1038/nn.2348

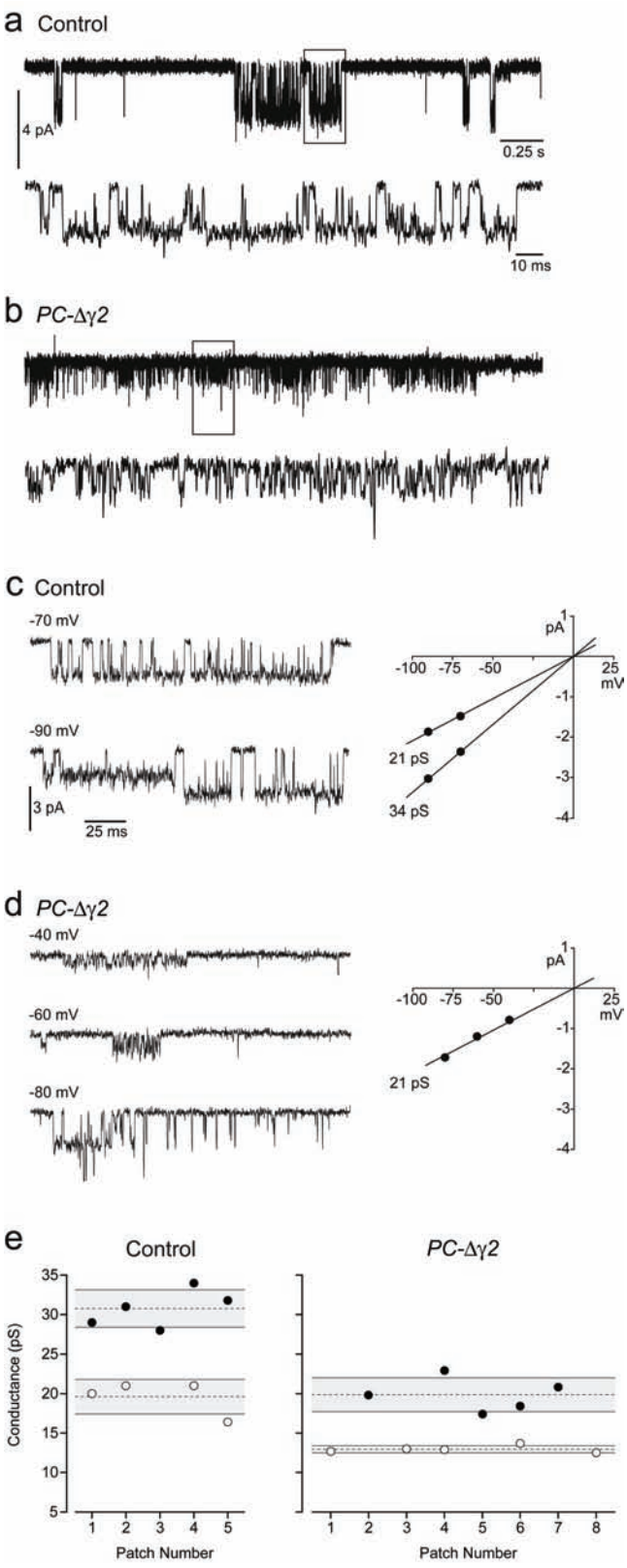

Figure S2 Purkinje cells of *PC-Δγ2* mice have extrasynaptic $GABA_A$ receptors characteristic of receptors lacking a γ2 subunit. (**a**) Single-channel events in an outside-out patch taken from a Purkinje cell of a control mouse (200 μM GABA, –70 mV); clusters of channel openings are separated by long closed periods. The lower trace is an expansion of the boxed region. All patches (n = 9) from control mice were responsive to GABA, and in the continued presence of GABA the

Nature Neuroscience: doi:10.1038/nn.2348

channels entered long-lived closed states characteristic of desensitization clusters[1]. (**b**) A recording of currents in a patch taken from a Purkinje cell of a *PC-Δγ2* mouse (–60 mV). All patches (n = 8) from *PC-Δγ2* mice were responsive to GABA (100-500 μM), often showing clear macroscopic responses on initial application, but the receptors exhibited a lower single-channel conductance and reduced desensitization. (**c**) Representative clusters from a single patch of a control Purkinje cell at two membrane voltages. To the right is the current-voltage relationship for this patch indicating the slope conductances of the two main conductance states observed. (**d**) Representative channel clusters recorded at three membrane voltages in a patch taken from a *PC-Δγ2* Purkinje cell. To the right is the corresponding current-voltage relationship. In this patch, and in 5 others, only a single main conductance state was detected; in 2 other patches two conductance states were present. (**e**) Plot showing the distribution of main conductance states among different patches from Purkinje cells of control and *PC-Δγ2* mice. Filled symbols represent the higher- and open symbols the lower conductance states. Dashed lines indicate the mean, and shaded areas the standard deviation, of conductance values from each group.

Methods: For single-channel recordings, GABA was applied at a high concentration (100-500 μM, typically 200 μM) sufficient to induce, in control patches, marked receptor desensitization. Under these conditions, $GABA_A$ receptors entered long-lived closed states, and channel openings occurred as infrequent clusters[1]. Such isolated clusters were analyzed to determine the main conductance states of the channels. In patches from *PC-Δγ2* mice, where receptor desensitization was reduced, single-channel activity was studied after equilibration with agonist for 30-60 s. Only one patch was recorded per cell. Whole-cell and single-channel currents recorded under such conditions were completely blocked by 10-20 μM of the $GABA_A$ receptor antagonist SR 95531.

Analysis: Single-channel currents from outside-out patches were analyzed by constructing all-point amplitude histograms (Fetchan; pCLAMP 8.1) from short selected epochs during which identified clusters of openings were present[1]. The mean single-channel current was determined from Gaussian fits to these amplitude distributions. Measurements were made at two or more potentials and the slope conductance estimated from the fit of the current-voltage relationship (assuming a reversal of 0 mV). In some patches, only single measurements of chord conductance were obtained; these were pooled with the slope conductance data to provide estimates of the single-channel conductance in each group of mice.

Nature Neuroscience: doi:10.1038/nn.2348

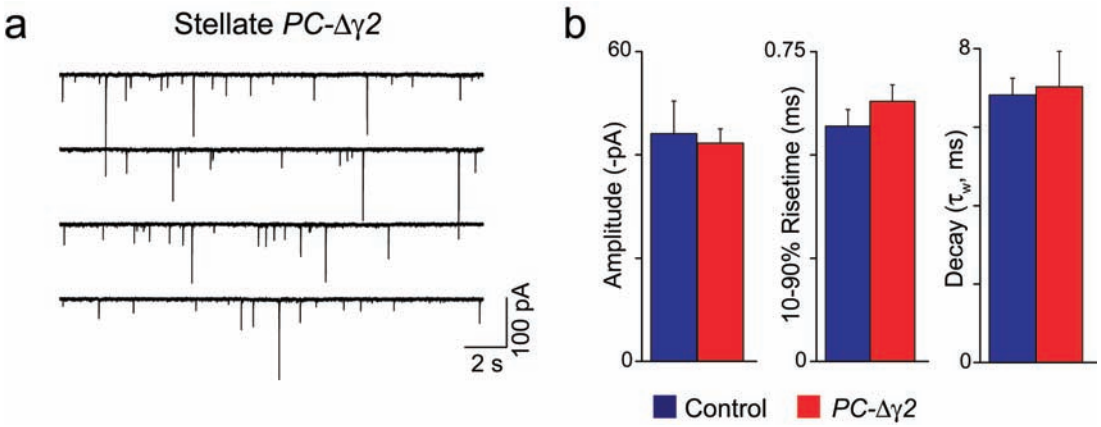

Figure S3 Loss of synaptic $GABA_A$ receptors in *PC-Δγ2* mice is restricted to Purkinje cells. (**a**) Contiguous segments of a recording in TTX from a molecular layer interneuron (presumptive stellate cell) of a *PC-Δγ2* mouse showing frequent mIPSCs. In the same cerebellar slice Purkinje cells were devoid of mIPSCs (as shown in **Fig. 2**). (**b**) Pooled data showing that the properties of molecular layer interneuron mIPSCs from control and *PC-Δγ2* mice did not differ (n = 4 and 5, respectively; peak amplitude p = 0.78, rise time p = 0.31, decay p = 0.85). Error bars denote s.e.m.

Nature Neuroscience: doi:10.1038/nn.2348

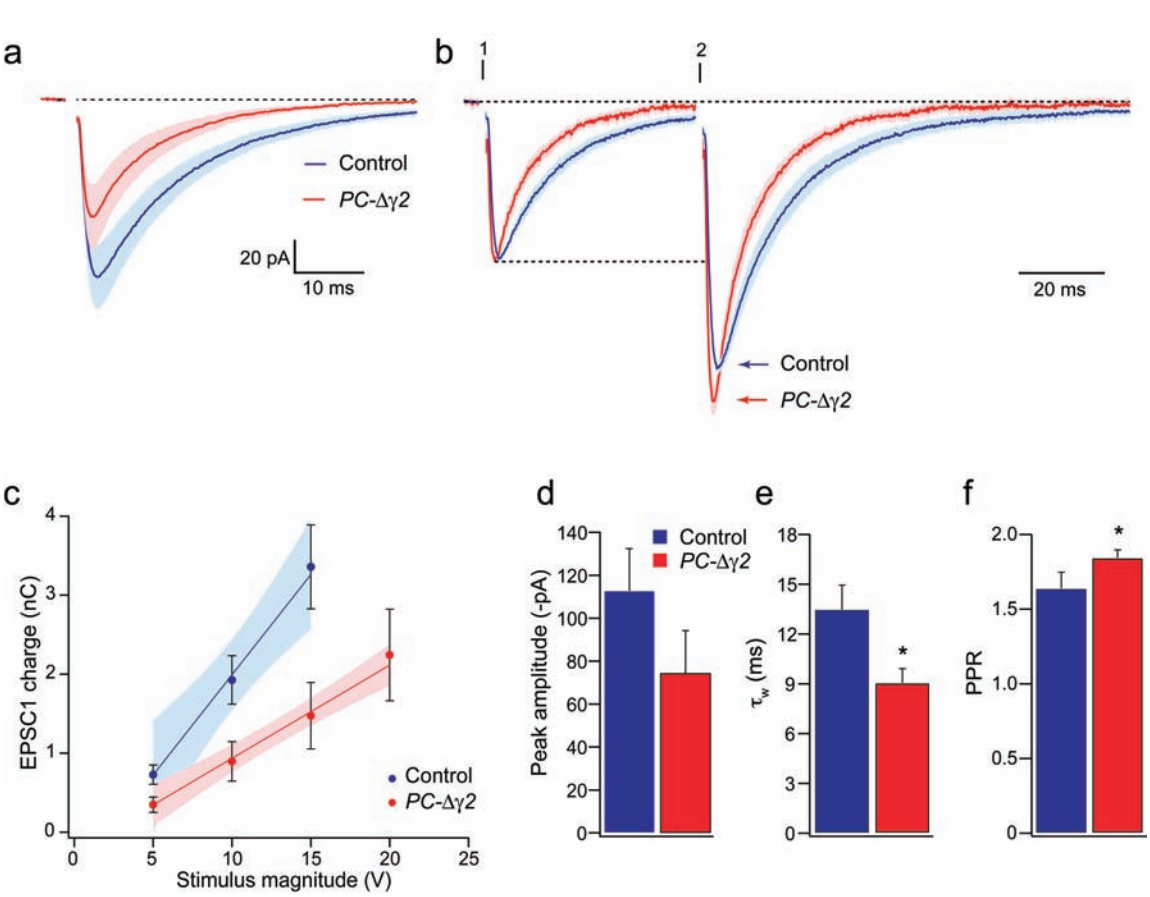

Figure S4 Parallel fiber-evoked excitatory input is altered in Purkinje cells lacking phasic synaptic inhibition. (**a**) Parallel fiber-evoked EPSCs (–60 mV) recorded from *PC-Δγ2* mice (red) and littermate controls (blue); traces show global averages and shaded areas represent ± s.e.m. (n = 14 and 13 cells, respectively). Dashed line illustrates the baseline current. (**b**) Paired parallel fiber-evoked EPSCs (–60 mV; 10 V stimulus, 50 ms interval); traces show global averages and shaded areas represent ± s.e.m. (n = 14 *PC-Δγ2* and 10 control cells). The average current was scaled to the peak of EPSC1. Dashed lines illustrate the baseline current and the peak of EPSC1. (**c**) Relationship between parallel fiber stimulus voltage (0.1 ms pulse duration) and EPSC1 charge transfer, for *PC-Δγ2* mice (red) and littermate controls (blue). Symbols denote mean, error bars denote s.e.m., and shaded areas the 90% confidence limits for the linear fits. The slopes of the fits are significantly different (p = 0.0025). **d**, **e** and **f**, Pooled data showing the peak amplitude (**d**), decay kinetics (τ_w) of EPSC1 (**e**) and PPR (**f**). Bars denote mean and error bars denote s.e.m.. Asterisks indicate significant differences (PPR p = 0.0099, Mann Whitney *U*-test; τ_w p = 0.018). For each cell, PPR was calculated as the mean of ratios (EPSC2/EPSC1) obtained at multiple voltages.

Methods: Paired PF-EPSCs were evoked by stimuli delivered with a glass pipette located within the molecular cell layer. Stimuli of 100 μs duration were delivered at 0.2 Hz, with a 50 ms paired-pulse interval. The stimulation intensity was varied pseudo-randomly in 5V steps (10 sweeps each voltage) (see also Ref. [2]). AMPAR-mediated PF-evoked EPSCs were recorded in the presence of strychnine (1 μM), SR-95531 (40 μM) and D-AP5 (50 μM) after 60-70% series resistance

Nature Neuroscience: doi:10.1038/nn.2348

compensation (typically 7 μsec lag-time). Recordings showing a >20 % increase of the series resistance were discarded. The peak current amplitude and the total charge transfer of averaged parallel fiber-evoked EPSCs were estimated (for a 10 V stimuli) using NeuroMatic.

Nature Neuroscience: doi:10.1038/nn.2348

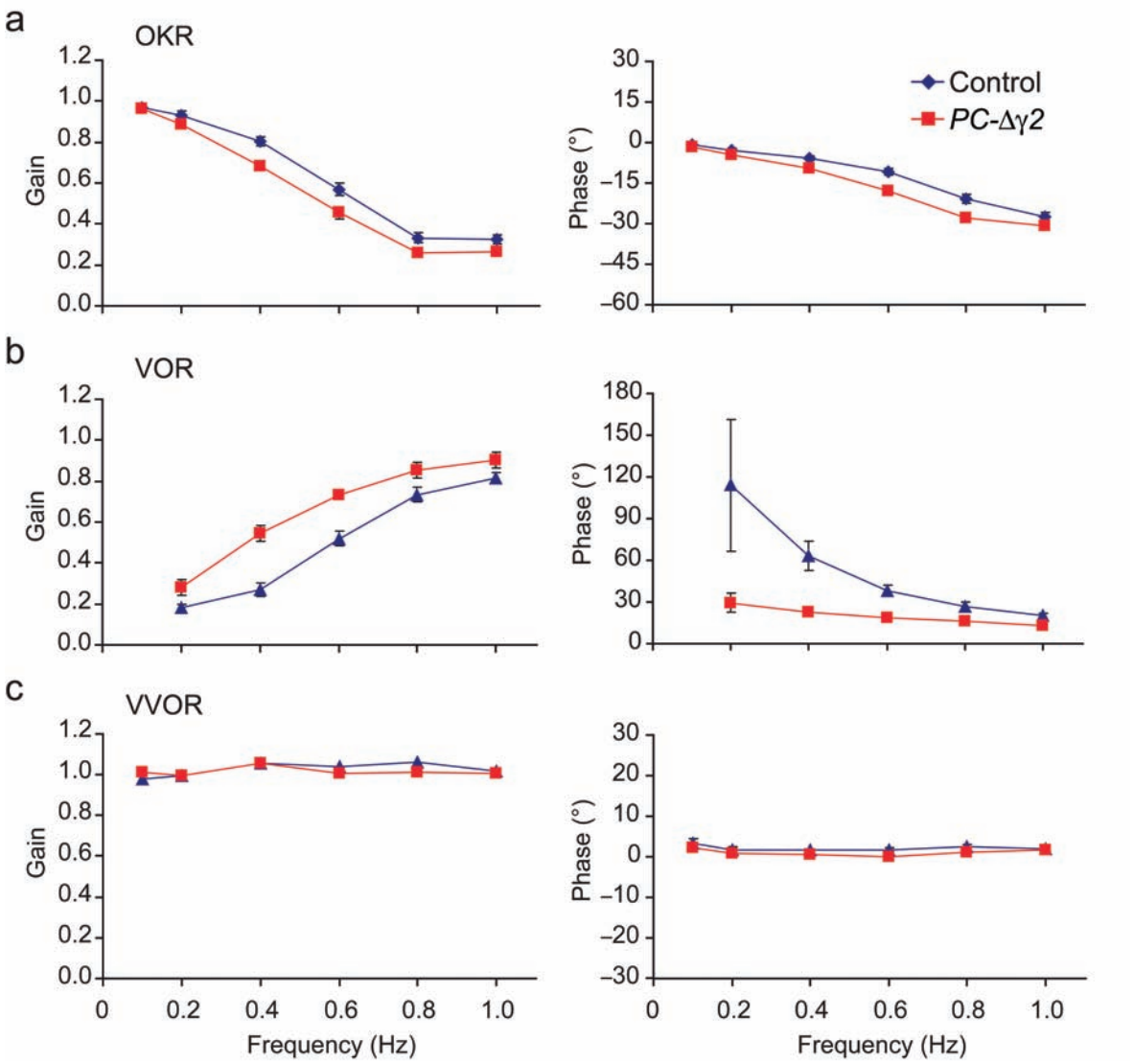

Figure S5 Motor performance during the optokinetic reflex (OKR) (**a**) and during the vestibulo-ocular reflex in the dark (VOR) (**b**) and the light (VVOR) (**c**). Stimulus frequencies of optokinetic drum and turntable were varied from 0.1 Hz to 1.0 Hz. Stimulus amplitude was fixed at 5° for both drum and table. Significant differences were observed between *PC-Δγ2* mice and controls in gain and phase during OKR ($p = 0.018$ and $p = 0.012$, respectively; two-way repeated-measures ANOVA) and VOR ($p = 0.012$ and $p = 0.030$), but not during VVOR ($p = 0.43$ and $p = 0.63$). Data are from 8 control and 9 *PC-Δγ2* mice. Vertical error bars denote s.e.m.

Nature Neuroscience: doi:10.1038/nn.2348

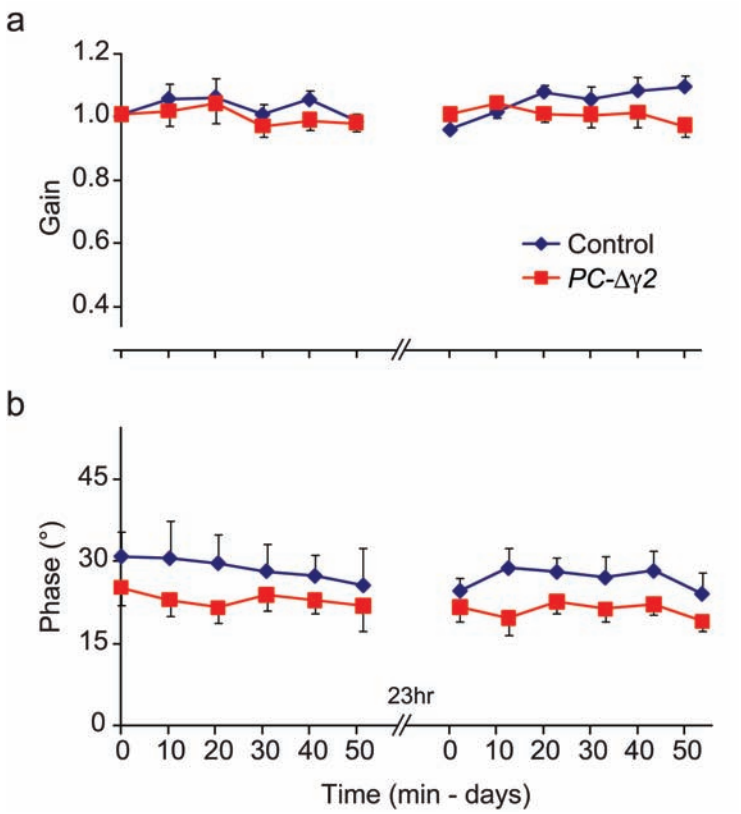

Figure S6 VOR gain decrease in *PC-Δγ2* mice results from the adaptation stimulus. VOR gain (**a**) and phase (**b**) were recorded in sessions with no adaptation-requiring stimulus (all other settings were the same as in experiments with such a stimulus). In this non-adapting paradigm, both control (n = 8) and *PC-Δγ2* (n = 9) mice show no significant changes in VOR gain over consecutive days. For both *PC-Δγ2* mice and controls, there was no difference between the last value of session 1 and the first value of session 2 (for *PC-Δγ2* mice p = 0.551 and for controls p = 0.610; paired Student's *t*-test). Moreover, for *PC-Δγ2* mice, first *vs* last value of session 1 p = 0.388 and first value of session 1 *vs* first value of session 2 p = 0.945; for controls these values are 0.518 and 0.328, respectively; paired Student's *t*-test. The lack of significant changes is markedly different from the results obtained during the actual adaptation sessions (see **Fig. 4**). Thus, VOR gain changes in *PC-Δγ2* mice following visuovestibular training result from the adaptation stimulus. Error bars denote s.e.m.

Nature Neuroscience: doi:10.1038/nn.2348

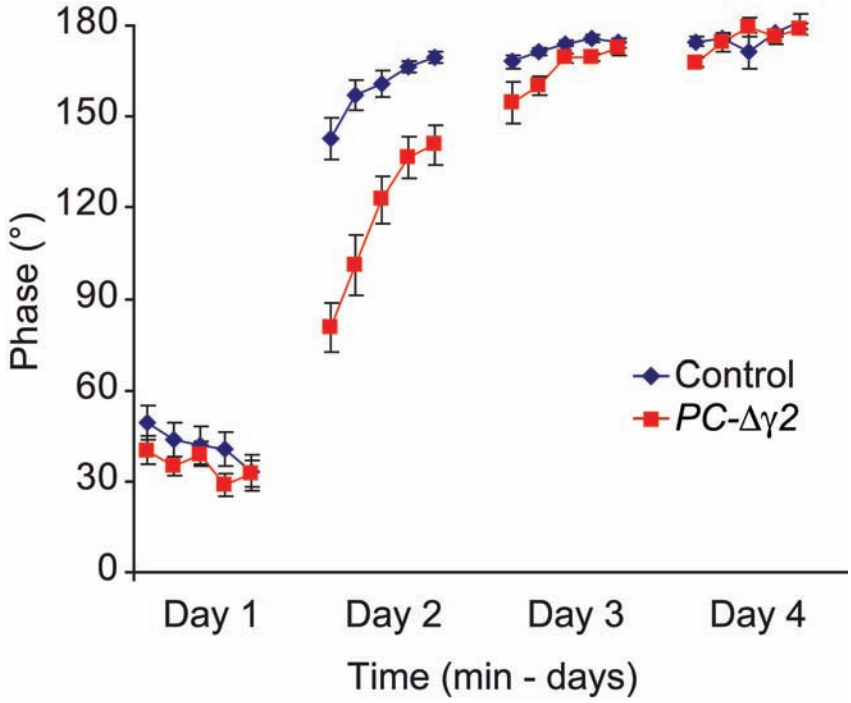

Figure S7 *PC-Δγ2* mice can reverse the phase during phase reversal training when measured in the light (VVOR training values). The phase changes show that *PC-Δγ2* mice were capable of perceiving the reversed movement of the visual stimulus on days 2-4. The reversed stimulus (starting on day 2) requires the eyes to move with a phase of 180°; this was fully achieved by all mice (control: n = 10; *PC-Δγ2*: n = 9) by the end of day 3. Error bars denote s.e.m.

Nature Neuroscience: doi:10.1038/nn.2348

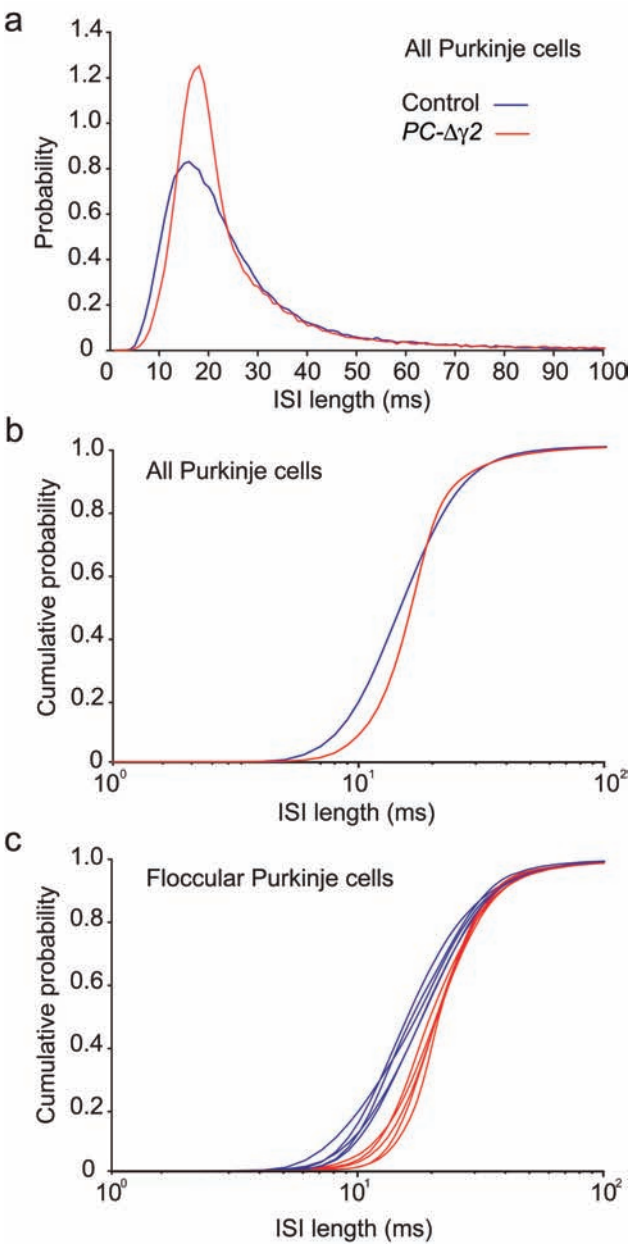

Figure S8 Simple spike ISI distributions are sharper in *PC-Δγ2* mice. (**a**) Histograms of individual ISI values pooled from all Purkinje cells recorded without any stimulus (control, blue, n = 63 cells; *PC-Δγ2*, red, n = 55 cells) indicate that *PC-Δγ2* Purkinje cell firing is focused more around a preferred interval, whereas in control mice the range of intervals is broader ($p < 0.001$, two-sample K-S test). (**b**) Corresponding cumulative probability histograms. The delayed rise and steeper slope indicate the relative absence of short intervals, and thus high frequency firing, in *PC-Δγ2* mice together with a relative abundance of 'normal' intervals. (**c**) Recordings from floccular Purkinje cells during compensatory eye movements evoked with visual stimulation demonstrate that this phenomenon is also present during motor performance. Shown are cumulative probability histograms of ISI values recorded with visual stimuli at various frequencies (0.1 – 1.6 Hz).

Nature Neuroscience: doi:10.1038/nn.2348

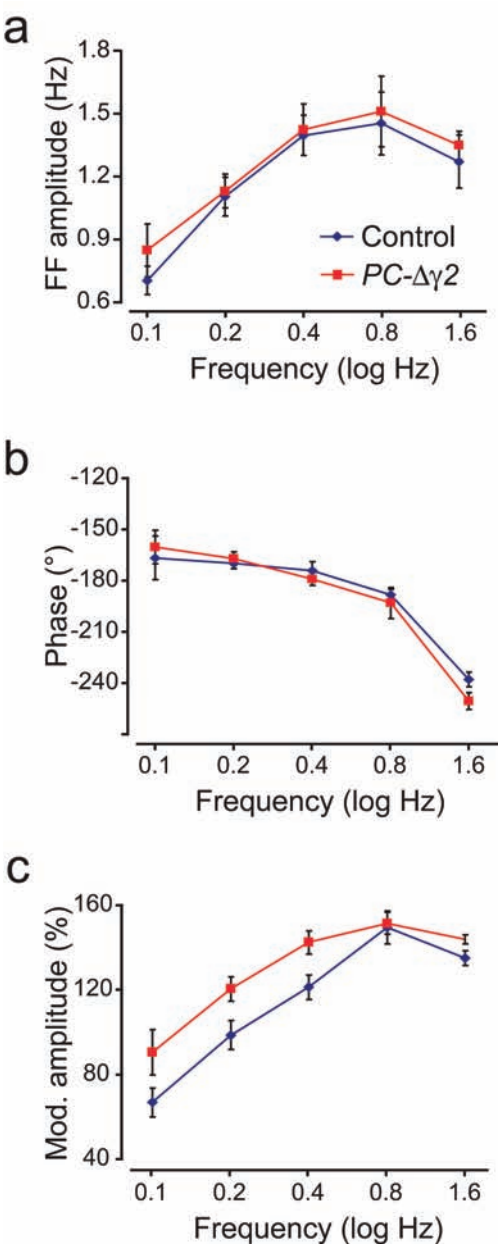

Figure S9 Removal of fast synaptic inhibition from *PC-Δγ2* Purkinje cells does not reduce climbing fiber responses to visual stimuli. Complex spike modulation was analyzed in a manner similar to that for simple spikes (**Fig. 5**). Modulation parameters were determined by fitting a sine wave through the peri-stimulus histogram. None of the parameters, including firing rate (**a**), phase (**b**) and modulation amplitude (**c**), were found to be significantly impaired in *PC-Δγ2* ($n > 8$ cells) compared to control mice ($n > 10$ cells); in fact, modulation amplitude was higher ($p < 0.02$) for 0.1 - 0.4Hz in *PC-Δγ2* mice. Error bars denote s.e.m.

Nature Neuroscience: doi:10.1038/nn.2348

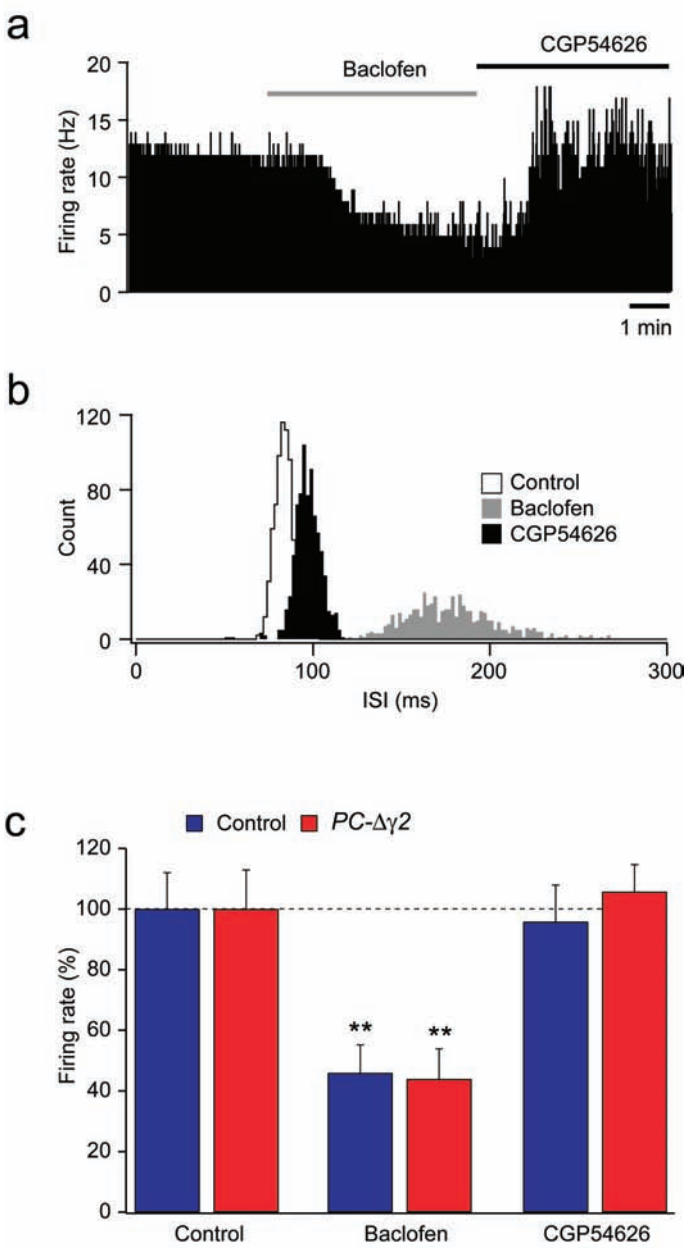

Figure S10 Baclofen reduces firing of Purkinje cells from both *PC-Δγ2* and control mice. (**a**) Firing rate record of a Purkinje cell in a slice from a control mouse in the presence of SR-95531 (20 μM), D-AP5 (20 μM), and 2,3-dioxo-6-nitro-1,2,3,4-tetrahydrobenzo[f]quinoxaline-7-sulfonamide (NBQX; 5 μM). Application of baclofen (10 μM; grey bar) caused a reduction in firing rate from 12 to 6 Hz. Subsequent addition of the $GABA_B$ antagonist CGP54626 (4 μM; black bar) restored firing to near control rates (10 Hz). (**b**) Histograms of inter-spike interval (ISI) for the cell shown in (**a**) (2 ms bin-width). ISI analysis was performed over ~1 min epochs at the end of the respective control or treatment period. (**c**) Pooled data showing the effect of baclofen in *PC-Δγ2* (n = 8) and control mice (n = 9), and the reversal of its actions by CGP54626. Baclofen reduced the firing rate to 43.9 ± 10.0% in *PC-Δγ2* mice ($p < 0.001$) and to 45.9 ± 9.3% in littermate control mice ($p < 0.005$). These changes in firing rate were not significantly different between the two groups of mice ($p = 0.89$). Moreover, restoring the firing rate by application of the $GABA_B$ receptor antagonist CGP54626 was

Nature Neuroscience: doi:10.1038/nn.2348

equally successful in *PC-Δγ2* and control mice. Firing rate was restored to 105.7 ± 9.0% in *PC-Δγ2* mice ($p = 0.71$) and to 95.8 ± 12.1% in control littermate mice ($p = 0.43$; Wilcoxon matched pairs test); these changes were not significantly different between the two groups of mice ($p = 0.17$; Mann-Whitney U test). Bars show mean and error bars s.e.m. Asterisks denote significant difference from control firing rate (** $p < 0.01$).

Nature Neuroscience: doi:10.1038/nn.2348

Simulation of VOR adaptation

Background

Several lines of evidence have indicated that the acquisition of cerebellar motor memory occurs through a form of 'system consolidation' that is characterized by different stages: memory formation is believed to take place initially in the cerebellar cortex, after which it is partly transferred to a downstream site for long-term consolidation during several days of ongoing training[3-5]. Likely candidate sites for consolidation are the deep cerebellar nuclei for the eyeblink and nictitating membrane response[4] and the vestibular nuclei for VOR adaptation[7], where regulation of plasticity could be instructed by specific modulation of inhibitory input that is learned by Purkinje cells[8]. This suggestion is supported by the various forms of intrinsic and synaptic plasticity that have been described in vestibular[9] and deep cerebellar nucleus neurons[10-13].

The model presented here represents a top-down description of an idealized VOR circuit, based on results from more elaborate modeling studies[14,15]. It simulates sinusoidal simple spike modulation of Purkinje cells, characterized by neural gain and phase relative to activation of the horizontal semicircular canals. Gain and phase values determine a 'position' on a polar plot, where 0^0 represents activation in phase with the ipsilateral canals. A similar description is applied to parallel fiber and interneuron activation, and to modulation of the neurons of the vestibular nucleus. Learning rules are implemented in a phenomenological way, as exponential decays towards a target gain or phase. The model covers 4 training cycles, each followed by a 'dark period'. During each training cycle, target gain and phase are set for a phase adaptation paradigm, as described in the **Methods**. Fast and slow phases of VOR adaptation are separated for simplicity. Adaptation during a training cycle is assumed to take place only in the cortex. During each 'dark period', the learned Purkinje cell signal becomes a target for adaptation in the vestibular nuclei, simulating 'systems consolidation'. Simultaneously, a partial extinction of cortical memory takes place during these periods.

Parallel fibers and interneurons

Parallel fibers are assumed to convey information from the ipsi- and contralateral labyrinth, with some phase dispersion. The majority of parallel fibers are assumed to display ipsilateral modulation. The same assumptions are applied to the signals conveyed by the interneurons. The gain of the Purkinje cell inputs at each phase $G_{in}(\phi)$ is described as Gaussian distributions centered on the ipsi- or contralateral input phase. Inhibitory and excitatory inputs are modeled to be present in equal number and strength (see **Fig. 6a**,**b**). The function of the parallel fiber and interneuron modulation in the simulation is to set the boundaries of the modulation depth that can be achieved by Purkinje cells. It is assumed that simple spike modulation can attain any 'position' on the polar plot within these boundaries through appropriate depression and potentiation of excitatory and inhibitory inputs.

Nature Neuroscience: doi:10.1038/nn.2348

Purkinje cells

The modulation of simple spike firing is assumed to be the result of linear summation of excitatory and inhibitory inputs[14,16]. The gain and phase of the modulation could be regulated through bidirectional plasticity of inhibitory and excitatory inputs[17-19]. In the case of symmetric excitatory and inhibitory inputs (as in **Fig. 6a**), the maximum attainable gain $G_{Pc}^{\max}$ for phase $\phi = 0$ (or 180) and $\phi = 90$ (or 270) can be found by vector summation:

$$G_{Pc0} = G_{Pc}^{\max}(\phi = 0) = 2\int_0^{90} G_{in}(\phi)\cos(\phi)d\phi$$

$$G_{Pc90} = G_{Pc}^{\max}(\phi = 90) = 2\int_0^{90} G_{in}(\phi)\sin(\phi)d\phi$$

These form the principle axes of an ellipse describing the maximum attainable gain $G_{Pc}^{\max}$ for each phase (**Fig. 6c**):

$$G_{Pc}^{\max} = \sqrt{\frac{G_{Pc0}^2 - G_{Pc90}^2}{\left[\left(G_{Pc0}/G_{Pc90}\right)\tan(\phi)\right]^2 + 1} + G_{Pc90}^2}$$

The absence of inhibition in *PC-Δγ2* mice results in an asymmetric gain distribution. In this case, $G_{Pc}^{\max}$ is a shifted ellipse (**Fig. 6c**). *PC-Δγ2* mice are assumed to have an impaired ability to express certain modulation phases at sufficient gain.

Vestibular nucleus

The manner in which excitation from mossy fiber collaterals and Purkinje cell inhibition is integrated in the floccular target neurons in the vestibular nuclei remains elusive. Considering the high baseline activity of vestibular first order afferents, Purkinje cells and second order vestibular neurons, a linear summation of rate coded excitatory and inhibitory inputs is used here, following the example of others[14,20]. The movement of the eyes is modeled to follow vestibular nucleus modulation rotated by 180°. Mossy fiber inputs are assumed to follow the ipsilateral canals ($\phi = 0^0$), such that the linear integration with Purkinje cell inhibitory input results in a shifted distribution of attainable gains at each phase of the eye movement relative to the head (**Fig. 6d**,**e**). Plasticity at the mossy fiber synapse[12,13] could determine the magnitude of the shift. Control mice can express VOR phases at higher gain than *PC-Δγ2* mice (**Fig. 6f**), and can even fully reverse the phase to 180°. Only ipsilateral (in phase with the ipsilateral canals) modulation of mossy fibers was considered here, but VOR phase reversal by adaptation to inputs arising from the contralateral labyrinth could give a similar outcome. In both cases, adaptation of mossy fiber input, combined with the available depth of modulation of simple spikes, determines the ability for phase reversal in the model.

Simulations

The simulation (**Fig. 6h**) describes four training sessions, each followed by an overnight period. Neural elements *Ne* are characterized by their gain and phase as *Ne=[phase,gain]*. Phase is

Nature Neuroscience: doi:10.1038/nn.2348

measured relative to activation of the semicircular horizontal canals; 0^0 means activation in phase with the ipsilateral primary afferents. Integration of inputs is performed by vector summations of the modulation of the neural elements in polar representation. The movement of the eyes *E* is given by a 180° rotation of the modulation of the vestibular nucleus *N* as $\vec{E} = -\vec{N}$. The modulation of the nucleus is calculated as a linear summation of excitatory mossy fiber *MF* and inhibitory Purkinje cell *Pc* inputs as $\overrightarrow{N} = \overrightarrow{MF} - \overrightarrow{Pc}$.

Training sessions

Each training session consists of an exponential decay of the system towards a target defined by the vestibular mismatch paradigm. The target phase and gain of the eyes $\vec{T}_{eye}$ is defined relative to head velocity. During a training session, the Purkinje cells adapt to the target defined as $\vec{T}_{Pc} = \vec{T}_{eye} + \overrightarrow{MF}$. If the target gain $\left|\vec{T}_{Pc}\right|$ exceeds the maximum attainable gain for this phase $G_{Pc}^{\max}$ (as defined above), the target gain is set to $\left|\vec{T}_{Pc}\right| = G_{Pc}^{\max}$.

The adaptation is governed by an exponential decay with time constant τ_{Pc}:

$$\tau_{Pc} \frac{d\overrightarrow{Pc}}{dt} = \vec{T}_{Pc} - \overrightarrow{Pc}$$

The slow and fast phases of VOR adaptation[12] are separated here so $\overrightarrow{MF}$ does not adapt during the training sessions.

Overnight period

During the overnight period two processes occur simultaneously: a partial extinction of the adapted modulation of the Purkinje cells and a 'systems consolidation' process through adaptation of the mossy fiber to vestibular nucleus input. The *Pc* extinction is modeled as a decay (as above), with the decay target set as a fraction γ_{Pc}^{decay} of the adapted state after the previous training session. This results in a decay of the gain, while preserving the phase.

The mossy fiber adaptation is modeled as a decay with time constant τ_{MF} towards a target $\vec{T}_{MF} = \overrightarrow{N} + \overrightarrow{Pc}$:

$$\tau_{MF} \frac{d\overrightarrow{Pc}}{dt} = \vec{T}_{MF} - \overrightarrow{MF}$$

Settings

Equations were numerically solved; each training session or overnight period consisting of 100 steps. Settings for **Fig. 6h** were chosen to approximately match the rate of adaptation to the experimental data.

Start conditions:

$$Pc = [180, 0.15],\ MF = [0, 0.85]$$

Nature Neuroscience: doi:10.1038/nn.2348

The conditions at the end of each period were used as start conditions for the next period.
Simulation settings for control mice:

$$\tau_{Pc} = 20\,,\tau_{MF} = 1.2\,,\gamma_{Pc}^{decay} = 0.3\,,G_{Pc0} = 0.5\,,G_{Pc90} = 0.25\,,G_{MF0} = 1$$

Simulation settings for *PC-Δγ2* mice, the same as control except:

$$\tau_{MF} = \infty\,,G_{Pc0} = 0.35\,,G_{Pc90} = 0.1$$

4-day phase adaptation paradigm:

$$\begin{aligned} T_{eye} = [&180, 0 \\ &30, 0.5 \\ &30, 1 \\ &30, 1] \end{aligned}$$

Nature Neuroscience: doi:10.1038/nn.2348

References

1. Brickley, S.G., Cull-Candy, S.G. & Farrant, M. Single-channel properties of synaptic and extrasynaptic $GABA_A$ receptors suggest differential targeting of receptor subtypes. *J Neurosci* **19**, 2960-2973 (1999).
2. Matsushita, K. *et al.* Bidirectional alterations in cerebellar synaptic transmission of tottering and rolling Ca^{2+} channel mutant mice. *J Neurosci* **22**, 4388-4398 (2002).
3. Kassardjian,C.D. *et al.* The site of a motor memory shifts with consolidation. *J. Neurosci.* **25**, 7979-7985 (2005).
4. Broussard,D.M. & Kassardjian,C.D. Learning in a simple motor system. *Learn. Mem.* **11**, 127-136 (2004).
5. Raymond,J.L., Lisberger,S.G. & Mauk,M.D. The cerebellum: a neuronal learning machine? *Science* **272**, 1126-1131 (1996).
6. Medina,J.F., Garcia,K.S. & Mauk,M.D. A mechanism for savings in the cerebellum. *J. Neurosci.* **21**, 4081-4089 (2001).
7. Lisberger,S.G. Neural basis for motor learning in the vestibuloocular reflex of primates. III. Computational and behavioral analysis of the sites of learning. *J. Neurophysiol.* **72**, 974-998 (1994).
8. Miles,F.A. & Lisberger,S.G. Plasticity in the vestibulo-ocular reflex: a new hypothesis. *Annu. Rev. Neurosci.* **4**, 273-299 (1981).
9. Gittis,A.H. & du Lac,S. Intrinsic and synaptic plasticity in the vestibular system. *Curr. Opin. Neurobiol.* **16**, 385-390 (2006).
10. Aizenman,C.D. & Linden,D.J. Rapid, synaptically driven increases in the intrinsic excitability of cerebellar deep nuclear neurons. *Nat. Neurosci.* **3**, 109-111 (2000).
11. Aizenman,C.D., Manis,P.B. & Linden,D.J. Polarity of long-term synaptic gain change is related to postsynaptic spike firing at a cerebellar inhibitory synapse. *Neuron* **21**, 827-835 (1998).
12. Pugh,J.R. & Raman,I.M. Potentiation of mossy fiber EPSCs in the cerebellar nuclei by NMDA receptor activation followed by postinhibitory rebound current. *Neuron* **51**, 113-123 (2006).
13. Zhang,W. & Linden,D.J. Long-term depression at the mossy fiber-deep cerebellar nucleus synapse. *J. Neurosci.* **26**, 6935-6944 (2006).
14. Masuda,N. & Amari,S.I. A computational study of synaptic mechanisms of partial memory transfer in cerebellar vestibulo-ocular-reflex learning. *J. Comput. Neurosci.* **24**, 137-156 (2007).
15. Medina,J.F. & Mauk,M.D. Simulations of cerebellar motor learning: computational analysis of plasticity at the mossy fiber to deep nucleus synapse. *J. Neurosci.* **19**, 7140-7151 (1999).
16. Miyashita,Y. & Nagao,S. Contribution of cerebellar intracortical inhibition to Purkinje cell response during vestibulo-ocular reflex of alert rabbits. *J. Physiol* **351**, 251-262 (1984).
17. Coesmans,M., Weber,J.T., De Zeeuw,C.I. & Hansel,C. Bidirectional parallel fiber plasticity

Nature Neuroscience: doi:10.1038/nn.2348

in the cerebellum under climbing fiber control. *Neuron* **44**, 691-700 (2004).

18. Rancillac,A. & Crepel,F. Synapses between parallel fibres and stellate cells express long-term changes in synaptic efficacy in rat cerebellum. *J. Physiol* **554**, 707-720 (2004).
19. Jorntell,H. & Hansel,C. Synaptic memories upside down: bidirectional plasticity at cerebellar parallel fiber-Purkinje cell synapses. *Neuron* **52**, 227-238 (2006).
20. Raymond,J.L. & Lisberger,S.G. Neural learning rules for the vestibulo-ocular reflex. *J. Neurosci.* **18**, 9112-9129 (1998).

Nature Neuroscience: doi:10.1038/nn.2348